

# Intranasal Delivery of BACE1 siRNA and Berberine via Engineered Stem Cell Exosomes for the Treatment of Alzheimer's Disease

Chunbin Sun<sup>1,\*</sup>, Shuang Sha<sup>1,\*</sup>, Yubang Shan<sup>1</sup>, Xiaoyu Gao<sup>1</sup> , Liang Li<sup>1</sup>, Cencan Xing<sup>1,2,\*</sup>,  
Zhongbao Guo<sup>3,\*</sup>, Hongwu Du<sup>1,2,\*</sup>

<sup>1</sup>School of Chemistry and Biological Engineering, University of Science and Technology Beijing, Beijing, 100083, People's Republic of China; <sup>2</sup>Daxing Research Institute, University of Science and Technology Beijing, Beijing, 100083, People's Republic of China; <sup>3</sup>China Testing & Certification International Group Co., Ltd, Beijing, 100024, People's Republic of China

\*These authors contributed equally to this work

Correspondence: Hongwu Du, School of Chemistry and Biological Engineering, University of Science and Technology Beijing, Beijing, 100083, People's Republic of China, Email hongwudu@ustb.edu.cn; Zhongbao Guo, China Testing & Certification International Group Co., Ltd, Beijing, 100024, People's Republic of China, Email gzb@ctc.ac.cn

**Introduction:** Alzheimer's disease (AD) is a common progressive and irreversible neurodegenerative disease. AD accounts for 60%–70% of all dementia cases, ranking as the seventh leading cause of death globally. Human umbilical cord mesenchymal stem cells (hUC-MSCs) characterized by their abundant availability and low immunogenicity, have demonstrated significant therapeutic potential for AD in both preclinical studies and clinical trials. The use of exosomes can help mitigate the issues associated with cellular therapies. However, the clinical application of hUC-MSCs remains challenging due to their inability to effectively traverse the blood-brain barrier (BBB) and reach pathological sites. Therapeutic strategies utilizing exosomes derived from hUC-MSCs (Exos) have emerged as an effective approach for AD intervention.

**Methods:** Here, we used ultrasound to construct multifunctional Exos (MseVB@R/siRNA) for AD therapy. We obtained small interfering RNA for  $\beta$ -site precursor protein lyase-1 (BACE1 siRNA) and berberine for co-delivery into the brain. Berberine, a classical anti-inflammatory agent, effectively alleviates neuroinflammation in AD pathogenesis. BACE1 serves as the pivotal cleavage enzyme in amyloid  $\beta$ -protein (A $\beta$ ) formation, where silencing BACE1 synthesis through BACE1 siRNA significantly reduces A $\beta$  production. In a 5xFAD mouse model, Exos selectively targeted microglial and neuronal cells after nasal delivery under the action of neural cell-targeting peptide rabies virus glycoprotein 29 (RVG29).

**Results:** BACE1 siRNA and berberine (BBR) loading enhanced the effectiveness of Exos in improving cognitive function, promoting nerve repair and regeneration, reducing inflammatory cytokine expression, and suppressing glial responses. BACE1 siRNA release was confirmed to reduce BACE1 expression and A $\beta$  deposition. Concurrently, berberine effectively suppressed the release of inflammatory factors, thereby reducing neuroinflammation.

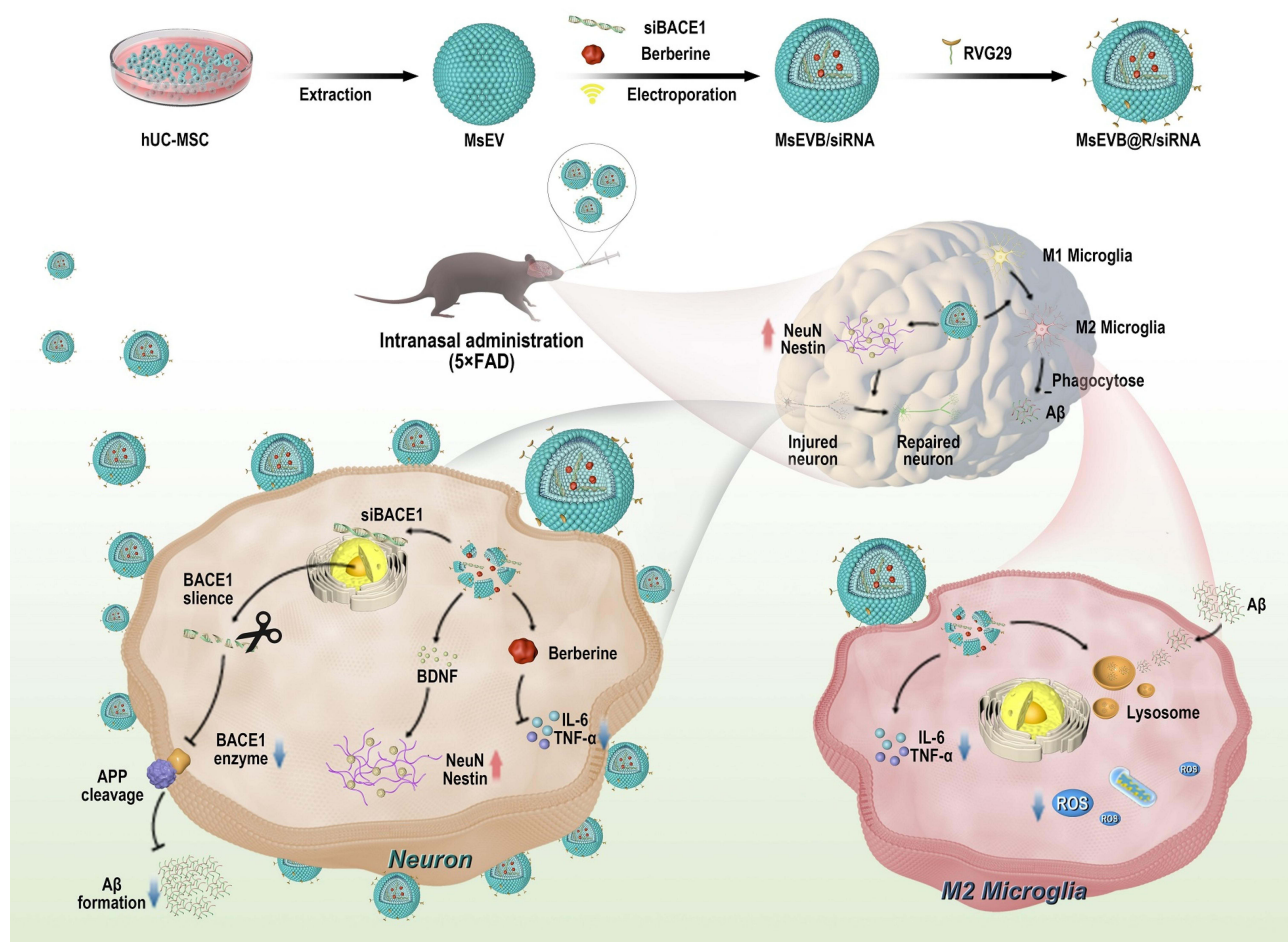
**Conclusion:** In conclusion, the nasal delivery of engineered exosomes is a potentially effective method for treating AD.

**Keywords:** Alzheimer's disease, engineering exosomes, intranasal delivery

## Introduction

Alzheimer's disease (AD) is a neurodegenerative disease characterized by cognitive dysfunction.<sup>1</sup> The primary pathological manifestations in patients with AD are amyloid  $\beta$ -protein (A $\beta$ ) deposition, neurofibrillary tangle formation, and neuroinflammation.<sup>2,3</sup> Currently, more than 55 million people worldwide are living with dementia. AD accounts for 60%–80% of all cases of dementia and is rapidly becoming one of the leading causes of disability and death among the elderly.<sup>4</sup> Projections indicate that AD-related healthcare expenditures will more than double by 2030, escalating from US 1.3 trillion annually in 2019 to US 2.8 trillion. The average annual medical expenditure for AD patients is threefold

## Graphical Abstract



higher than that of non-AD individuals, necessitating long-term care.<sup>5</sup> Furthermore, AD leads to workforce attrition and imposes substantial strain on social welfare systems. The disease also causes progressive memory loss and language impairment, severely compromising verbal communication abilities. AD patients face elevated risks of complications such as dysphagia and infections secondary to prolonged bed rest.<sup>6</sup> Current clinical therapeutics for AD include cholinesterase inhibitors (eg, donepezil), N-methyl-D-aspartic acid receptor (NMDA) receptor antagonists (eg, memantine), and monoclonal antibodies like lecanemab. However, the therapeutic outcomes of currently available AD medications remain suboptimal.<sup>7</sup> One of the principal contributors to this is the inherent blood-brain barrier (BBB). The BBB protects the brain from harmful substances and pathogens circulating in the blood, maintains a healthy microenvironment, and prevents most drugs from reaching the brain. This structure poses a major challenge in drug delivery for treating of brain diseases. Concurrently, developing drugs that inhibit Aβ production has faced multiple challenges.<sup>8,9</sup> Compared with monotherapy, intranasal delivery of exosomes for AD treatment demonstrates enhanced therapeutic efficiency through improved drug bioavailability and reduced dosage requirements. This modality additionally alleviates hepatic and renal metabolic burdens associated with systemic drug administration.<sup>10,11</sup> Moreover, the non-invasive nature of nasal administration simplifies clinical procedures, reduces healthcare costs, and improves cost-effectiveness.<sup>12,13</sup> Therefore, in addition to continuous investigations on the mechanisms underlying AD, the development of multi-target directed ligand strategies (MTDLS) and one-compound multi-target strategies has great prospects in treating AD.

Cellular exosomes (Exos) are nanoparticles produced by most cells and serve as intercellular transport vehicles for biomolecular cargo from host cells to recipient cells.<sup>14</sup> Stem cell-derived Exos have garnered considerable attention owing to their unique properties: less than 200 nm in diameter, they can easily bypass the BBB and protect their contents from degrading lipid biofilms. The abundant biomolecules derived from stem cells, including nucleic acids and metabolites may serve as alternatives to cellular therapeutics.<sup>15,16</sup> Evidence suggests that Exos is a major component of transplanted MSCs in AD treatment. Compared to MSC,<sup>17,18</sup> MSC-derived Exos has significant advantages, such as cell-free structure, low immunogenicity, specific and convenient delivery route, and ability to carry drugs, making it a suitable alternative for the MSC-based treatment of neurological diseases. Exos may play various roles in AD neuroinflammation, inhibition of A $\beta$  production, nerve regeneration, and axon reconstruction.<sup>19,20</sup> To target BBB penetration, nanoparticles capable of receptor-mediated endocytosis are designed to penetrate the BBB and treat brain diseases when administered intravenously. However, owing to the rapid clearance and metabolic changes in the systemic circulation, these drugs are cleared before they can be recognized by the receptor on the BBB, which further reduces the efficiency of the drugs. Thus, intranasal administration is a noninvasive and safe method for drugs to bypass the BBB and directly enter the brain via olfactory nerve axons or connective tissue surrounding the olfactory tract. Recent studies have shown that Exos can reach the hippocampus and play a neuroprotective role in the hippocampus when administered via the nasal route.<sup>21,22</sup>

AD involves multiple etiologies, including but not limited to A $\beta$  deposition and neuroinflammation. A $\beta$  is expressed at high levels in the brain of patients with AD and aggregates into toxic oligomers and fibers produced by the beta-secretase cleavage of amyloid precursor protein (APP). These aggregations trigger events that lead to neuronal damage and necrosis.<sup>23</sup> In addition, the disease-related state of microglia M1 exacerbates neuroinflammation in the brain, impeding the clearance of toxic substances, including A $\beta$  and tau, and further aggravates the disease.<sup>24,25</sup> Combination drugs that block these pathways help slow the progression of AD. Small interfering RNA for  $\beta$ -site APP lyase-1 (BACE1 siRNA) downregulates the expression of  $\beta$ -secreting enzyme and reduces the synthesis of A $\beta$  from the source. The inflammation suppressant berberine is then delivered in combined form in the microglia to suppress the cellular inflammatory state and help clear A $\beta$  and tau proteins. Due to its anti-inflammatory effects, berberine can reshape the inflammatory microenvironment and alleviate AD symptoms.<sup>26</sup>

## Materials and Methods

### Materials

Cy7 and Cy5 NHS esters were purchased from Dalian Meilun Biotechnology Co., LTD. (Dalian, China). A $\beta$  (1–42) peptide (A $\beta$ 1–42) and FITC-A $\beta$  were purchased from GLS Biological Chemical Co., LTD. (Shanghai, China). BACE1 siRNA (sense: GCUUGUGGAUGGUGGUGATT, antisense: UCCACCAUCUCCA AAGCTT) and negative control siRNA (sense: UUCUCCGAACGUGUCA CGUT, antisense: ACGUGACACGUUCGGAATT) were purchased from Ractigen Therapeutics (Jiangsu, China). Berberine was acquired from Durst Biotechnology Co., LTD. (Chengdu, China). CD9 Rabbit Monoclonal Antibody (AG1418, Beyotime, China), CD63 Rabbit Monoclonal Antibody (AF1471, Beyotime, China), TSG101 Mouse Monoclonal Antibody (AG3472), Anti-amyloid 1–42 antibody, anti-IL-6 antibody, anti-TNF- $\alpha$  antibody, anti-NEUN antibody, and anti-Nestin antibody were purchased from China Servicebio Technology CO., LTD. All chemicals used were of analytical or reagent grade.

### Cells and Animals

BV-2 and SH-SY5Y cell lines were purchased from the Cell Bank of the Chinese Academy of Sciences (Shanghai, China). 5xFAD mice were purchased from Cavens Laboratory Animal Co., LTD. (Changzhou, China). All animals were kept under standard conditions. Water and food were freely available under typical housing conditions (room temperature 22°C  $\pm$  2°C, humidity 55%  $\pm$  10%) with a 12-hour light/12-hour dark cycle. Male 5xFAD mice (six months) were randomized into the model and treated groups; the wild-type mice were used as the negative control (n = 6). Mice in each group received intranasal administrations twice weekly over a 4-week treatment period. Each administration session comprised four sequential instillations of exosomes (1 mg/mL), with 5  $\mu$ L aliquots delivered over 10-second intervals at

2 min pauses, totaling 20  $\mu\text{L}$  per session. Animal experiments were conducted according to the guidelines established and approved by the Laboratory Animal Management Committee of Yunnan Best Biotech Co., LTD. The assigned approval number is BST-MICE-PZ-20230609-1.

## Cell Viability Assay

Cell viability was assessed using the Cell Counting Kit-8 (CCK8) (Beyotime Biotech). After the cells showed 80% fusion in 96-well plates, different concentrations of MsEV, MsEVB/siRNA, and MsEVB@R/siRNA were added to the medium, and the cells were cultured for 24 h. Two hundred microliters of CCK8 working solution were added to each cell. The cells were incubated in the solution for 2 h, rinsed twice with phosphate-buffered saline (PBS), and the cells added to the medium. The absorbance of the supernatant in each sample at 450 nm was measured using enzyme-labeling method.

## Preparation of Exosomes

The human umbilical cord stem cell supernatants were collected and centrifuged at  $300 \times g$  and  $2000 \times g$  for 10 min to remove cells and cell debris. The resulting supernatant was centrifuged at  $10000 \times g$  at  $4^\circ\text{C}$  for 30 min to remove debris. The final supernatant was centrifuged at  $100,000 \times g$  for 70 min. The step was repeated twice to obtain the exosome precipitate. The obtained exogenic material was suspended in fresh PBS.

## Cellular Uptake

The cells were cultured in DMEM supplemented with 10% fetal bovine serum and 1% double antibody culture medium at  $37^\circ\text{C}$  in 5%  $\text{CO}_2$ . Cy5 and exosomes were preincubated at  $37^\circ\text{C}$  for 1 h to prepare Cy5-labeled exosomes. SH-SY5Y and BV2 cells were inoculated in confocal petri dishes at  $1 \times 10^4$ /well density. MsEV, MsEVB/siRNA, and MsEVB@R/siRNA were added to the Petri dish and incubated for 2 h and 4 h, respectively. After incubation, the culture dish was washed three times with PBS, dyed with 0.5  $\mu\text{g}/\text{mL}$  phalloidin solution for 5 min, washed three times with PBS, dyed with 0.5  $\mu\text{g}/\text{mL}$  DAPI solution for 5 min, washed again with PBS, and observed under a confocal microscope (Leica TCS SP 5, leica, Germany).

## Nano Tracking Analyzer (NTA) Assay

The sample was diluted 1000 times with PBS according to the protein concentration of the sample, following which the particle size/particle concentration/membrane potential was determined. First, the standard product was diluted 250,000 times with PBS for future use. The instrument and corresponding software were used. After the self-testing of the instrument was completed, a 20 mL syringe was used to gradually add approximately 10 mL of PBS into the instrument, following which approximately 5 mL of the standard was used to calibrate the instrument. After instrument calibration, 5 mL of PBS was added, the standard was rinsed, 5 mL of the sample was added, and the test was conducted. After the test was completed, the test data were saved, and the instrument was cleaned with PBS for future use.

## MRI Imaging in vivo

MsEV, MsEVB/siRNA, and MsEVB@R/siRNA were incubated with Cy7 at  $37^\circ\text{C}$  for 1 h, following which the unbound dyes were eluted using ultrafiltration tubes. Six-month-old 5xFAD mice were injected with 10  $\mu\text{L}$  of Cy7-labeled exosomes by nasal drip. The fluorescence intensity in the brain of mice was measured using a multi-functional imaging system at 1, 3, 6, 12, and 24 h. After the experiment, the tissues and organs were scanned to calculate the fluorescence intensity.

## Hematoxylin and Eosin Staining

Brain tissues were fixed in 4% paraformaldehyde for 24 h, paraffin -embedded, and then sliced. The slices were successively added to xylene I for 20 min, xylene II for 20 min, anhydrous ethanol I for 5 min, anhydrous ethanol II for 5 min, and 75% alcohol for 5 min. The slices were immersed in hematoxylin and stained for 5 min, washed with PBS, rinsed with PBS after differentiation with a hydrochloric acid solution, treated with an ammonia solution (upon which

they turned blue), and washed with PBS. The sections were dehydrated in an alcohol gradient and then stained in eosin solution for 5 min. Following this, the slices were treated with anhydrous ethanol I for 5 min, anhydrous ethanol II for 5 min, anhydrous ethanol III for 5 min, n-butanol for 5 min, xylene I for 5 min, and xylene II for 5 min. The slices were removed from xylene, dried partially, and then sealed. The experimental results were observed under a microscope, and image data were collected and analyzed.

## Immunofluorescence

The slices were successively dehydrated in a dewaxing solution and anhydrous ethanol and then rinsed with ddH<sub>2</sub>O. The tissue sections were then placed in a repair box containing Ethylenediaminetetraacetic acid (EDTA) antigen repair buffer (pH 8.0) for antigen repair. The slide was placed in PBS (pH 7.4) and washed three times under shaking conditions on a decolorizing shaker for 5 min. After the sections dried partially, a tissue pen was used to draw a circle around the tissue, and bovine serum albumin (BSA) was added to the circle and incubated for 30 min. PBS was added to the slices along with a certain proportion of primary antibody, and the slices were placed flat in a wet box at 4°C and incubated overnight. The slides were then placed in PBS (pH 7.4) and washed three times under shaking conditions in a decolorizing shaker for 5 min. After the slices had dried partially, a tissue coated with the secondary antibody labeled with the corresponding species of the primary antibody in a certain proportion was added to the ring and incubated at room temperature for 50 min. After the slices had dried partially, DAPI was added to the circle, and the sample was incubated for 10 min at 37°C in the dark. The ring was treated with a quenching agent for 5 min, and the water was washed for 10 min. The slides were placed in PBS (pH 7.4) and washed three times under shaking conditions in a decolorizing shaker for 5 min. The tablets were sealed with anti-fluorescence quenched tablets. The sections were placed under a scanner for image acquisition or a fluorescence microscope.

## Morris Water Maze (MWM) Experiment

During the experimental period, the water temperature was maintained at approximately 20 to 21°C, and cards of different shapes and colors were marked in the four quadrants of the water maze for orientation reference. The four quadrants of the water maze were marked with cards of different shapes and colors as orientation references. On the first day of the experiment, the platform was set to be visible at 1 cm above the water level. Water was added to the platform, flags were placed on the platform, and the mice were trained to find the platform more easily. If the mice did not find a platform within 60s, they were placed on it for 15s, dried, and returned to the cage. The experiment was repeated to ensure that it commenced from a different entrance (quadrant) at each instance. Mice with eye diseases and mobility challenges were excluded, and mice that found the platform within a consistent period on the first day were selected for follow-up experiments. On days 2 to 5 of the experiment, water was injected into the water maze, the platform was submerged 1 cm below the water level, and white pigment was added to assess the learning ability of the mice. The mice were allowed to move freely in the water maze for 60s, and their quadrantal activity time and trajectory were recorded and analyzed using Super-Maze software. On day 6 of the experiment, the platform was removed, the mice were placed from the farthest end of the platform, and the mice could move freely for 60s. Software analysis investigated the long-term memory of the mice. The detection indexes included incubation period(s), total duration(s), total distance (mm), and the number of platform crossings.

## New Object Regeneration (NOR)

The mice were placed in a NOR box to familiarize them with their environment. The NOR box contained two identical objects that the mice could explore freely for 6 min, and their activity was recorded. The mice were then removed and placed in the cage to rest for 1 h. An object in the NOR box was replaced with a new object with a different shape and color but a similar size. Following this, the mice were again placed in the NOR box and allowed to explore the box for 6 min freely. The time the mice spent exploring the new and the old objects (placed within 2 cm of the object) was recorded. The duration of exploration was calculated when the distance between the mouse's nose and the object was less than 1 cm or when the mouse directly touched the object with its nose.

## Structure of MsEVB@R/siRNA

The outer cut was loaded and placed in a copper mesh for 3–5 min. After staining with 2% (w/v) phosphotungstic acid for approximately 2 to 3 min, the sample was washed twice with PBS. The images of MsEVB@R/siRNA with and without berberine and siRNA were obtained using the JEM-1400 transmission electron microscope (JEOL) at an accelerated voltage of 120 kV.

## Western Blot Analysis

The levels of CD9, CD63, TSG101, and GAPDH proteins were detected by Western blotting. hUC-MSC cells and exosomes were collected, cellular and Exos proteins were extracted, and the protein concentrations were measured using a NanoDrop instrument. The total protein cleavage product per well was separated by 12% sodium dodecyl sulfate-polyacrylamide gel and then transferred to a PVDF membrane. Anti-CD9 (1:1000 dilution), anti-CD63 (1:1000 dilution), anti-TSG101 (1:1000 dilution), and anti-GAPDH (1:2000 dilution) antibodies were used as the primary antibodies. Images were recorded using the GeneGnome XRQ Chemiluminescence Imaging System (SYGNO104187, Syngene). The gray level of the image was quantified using GeneTools.

## Transcriptomic Analysis

According to the manufacturer's instructions, RNA was extracted from mouse brain tissue, and mRNA with poly A structure was enriched using Oligo(dT) magnetic beads in total RNA. RNA was divided into fragments of approximately 300 bp by ion interruption. Using RNA as a template, 6-base random primers and reverse transcriptase were used to synthesize first-strand cDNA, and second-strand cDNA was synthesized using the first-strand cDNA as a template. After the library was constructed, PCR amplification was used to enrich the library fragments. Following this, the library was selected according to the fragment size, which was 450 bp. Following this, the library was examined using an Agilent 2100 Bioanalyzer, and the total concentration and effective concentration of the library were measured. Following this, according to the effective concentration of the library and the data required for the library, the libraries containing different index sequences were mixed proportionally. The hybrid library was uniformly diluted to 2 nM, and a single-strand library was formed using alkali denaturation. After RNA extraction, purification, and library construction, the libraries were subjected to paired-end (PE) sequencing by next-generation sequencing (NGS) using the Illumina sequencing platform. Raw data were filtered, and the filtered high-quality sequence (clean data) was compared to the reference genome of the species. According to the comparison results, the expression of each gene was calculated. Based on this, the samples were further analyzed by expression difference, enrichment, and cluster analyses. The transcript sequences were reconstructed by splicing the above reads.

## Loading of Berberine, siRNA and RVG29 Into Exosomes and Their Evaluation

Berberine and BACE1 siRNA were loaded in MsEV using the ultrasonic method. The loading efficiency was calculated by the liquid phase. In brief, for ultrasonic drug delivery to exosomes, BACE1 siRNA (1:10), berberine, and exosomes (1:1) were mixed and subjected to ultrasound (20% amplitude, six cycles, 30 s on/150 s off). After ultrasound, berberine, BACE1 siRNA, and exosome solutions were incubated at 37°C for 60 min to obtain MsEVB/siRNA. RVG29 was incubated with MsEVB/siRNA at 37°C to obtain MsEVB@R/siRNA. Sephadex G25 was used to separate excess free drugs in MsEVB@R/siRNA by volume exclusion chromatography. For further validation, the samples were prepared in high-performance liquid chromatography (HPLC)-grade methanol and analyzed using an internal control on the Agilent 1290 (Agilent Technologies) UHPLC system. Chromatography was performed on a C18 column (1.7  $\mu$ m 2.1 $\times$ 100 mm) using 2 mL of the samples. The column temperature was 40°C, and the mobile phases were 0.1% formic acid (A) and 0.1% formic acid (B). The flow rate was 0.1 mL/min. MS and MS/MS data were retrieved using the Agilent 6540 Q-TOF mass Spectrometer (Agilent Technologies), equipped with a positive ion mode jet ESI source. The Mass Hunter (Agilent Technologies) B.03 software was used to analyze the data. The mass spectrum data were analyzed in the 100e1700 m/z range for all mass spectrum peaks.

## Flow Cytometry

BV2 cells were inoculated in six-well plates with a density of  $1 \times 10^6$ . BV2 cells were pretreated with A $\beta$ 42 oligomerization for 12 h. Subsequently, BV2 cells were incubated with MsEV, MsEVB/siRNA, and MsEVB@R/siRNA for 24 h, respectively. After digestion centrifugation and PBS rinse twice, the cells were stained with CD86 and CD206 flow antibodies (1:500) according to the manufacturer's instructions. Then, the cells were washed three times with PBS, collected, and suspended in PBS for flow cytometry assay.

## Statistical Analysis

Statistical analysis was performed using GraphPad Prism 9.0.0. The graphs showed the mean  $\pm$  SD, unless otherwise specified. A two-tailed unmatched *t*-test was used to compare between two groups, and a one-way analysis of variance was used for comparison between multiple groups. NS indicated "no statistical significance" whereas  $p < 0.05$  indicated statistically significant differences.

## Results

### Preparation and Identification of Engineered hUC-MSC Exosomes

In the brain, the hippocampus is crucial for learning and memory and is particularly vulnerable in the early stages of AD progression. Alterations in hippocampal neurogenesis represent a key event in the early years of AD.<sup>27</sup> The low immunogenicity of stem cell exosomes makes them suitable as drug delivery carriers because they are better internalized by recipient cells.<sup>28</sup> We used exosomes derived from human umbilical cord mesenchymal stem cells as drug delivery and therapy carriers. As previously mentioned, A $\beta$ , which is involved in the pathogenesis of AD, is synthesized by the cleavage of APP by  $\beta$ -secretase, and BACE1 siRNA can downregulate the expression of  $\beta$ -secretase and suppress the synthesis of A $\beta$ .<sup>29</sup> We introduced BACE1 siRNA, berberine, and RVG29 into hUC-MSC exosomes by ultrasound. Next, we characterized the size distribution, morphology, membrane potential, CD9, CD63, and TSG101 (exosome labeling) of MsEVB@R/siRNA. TEM results showed no significant differences in exosome morphology between untreated exosomes and ultrasound-loaded drugs. Results obtained with the NTA showed that the size of the exosomes was 115 nm originally, and the size of the exosomes after drug loading was approximately 170 nm, indicating that the drugs were successfully loaded in the exosomes (Figure 1A and C). The minor changes in the Zeta potential and membrane properties indicated that the surface charge of the exosome was unaffected by the engineering process (Figure 1B). Western blotting and further quantitative analysis confirmed that compared with those in hUC-MSC cells, the expression levels of CD9, CD63, and TSG101 exosome marker proteins in Exos were significantly increased, suggesting the successful extraction of Exos (Figures 1D and S1B). The berberine content in the Exos measured by the Liquid chromatography method was approximately 14.8  $\mu$ g/mL (Figure 1E). After 48 h, the cumulative release rates of MsEVB/siRNA and MsEVB@R/siRNA were 89.6% and 92.4%, respectively (Figure 1F). Immunofluorescence results showed that 24 h after the intervention with BACE1 siRNA-loaded exosomes in APP-overexpressing SH-SY5Y cells, the expression level of A $\beta$  in the cells reduced significantly. mRNA detection showed consistent results, indicating successful BACE1 siRNA loading (Figures 1G and H; S1A). To determine the effects of MsEV, MsEVB/siRNA, and MsEVB@R/siRNA on the activity of nerve cells and microglia, SH-SY5Y cells, and microglia were treated with cell culture medium, MsEV, MsEVB/siRNA, and MsEVB@R/siRNA in 96-well plates. The survival rate of the cells was measured after 24 h of culture (Figure 1I and J). MsEV, MsEVB/siRNA, and MsEVB@R/siRNA did not inhibit cell proliferation, suggesting that exosomes may be a suitable vector for AD therapy.

### Engineered hUC-MSC Exosomes Can Effectively Reduce Nerve Injury and Suppress Microglial Inflammatory Responses

We assessed the ability of MsEVB@R/siRNA to be internalized by nerve cells overexpressing APP. MsEVB@R/siRNA could be taken up by nerve cells after co-incubation with the cells for 6 h (Figure S2A). Next, we assessed the ability of MsEVB@R/siRNA to produce A $\beta$  in APP-overexpressing nerve cells (SH-SY5Y<sup>APP</sup>). Compared with the Model group, the A $\beta$  level in the MsEVB@R/siRNA was significantly lower, and IL-6 and TNF- $\alpha$  protein expression were significantly

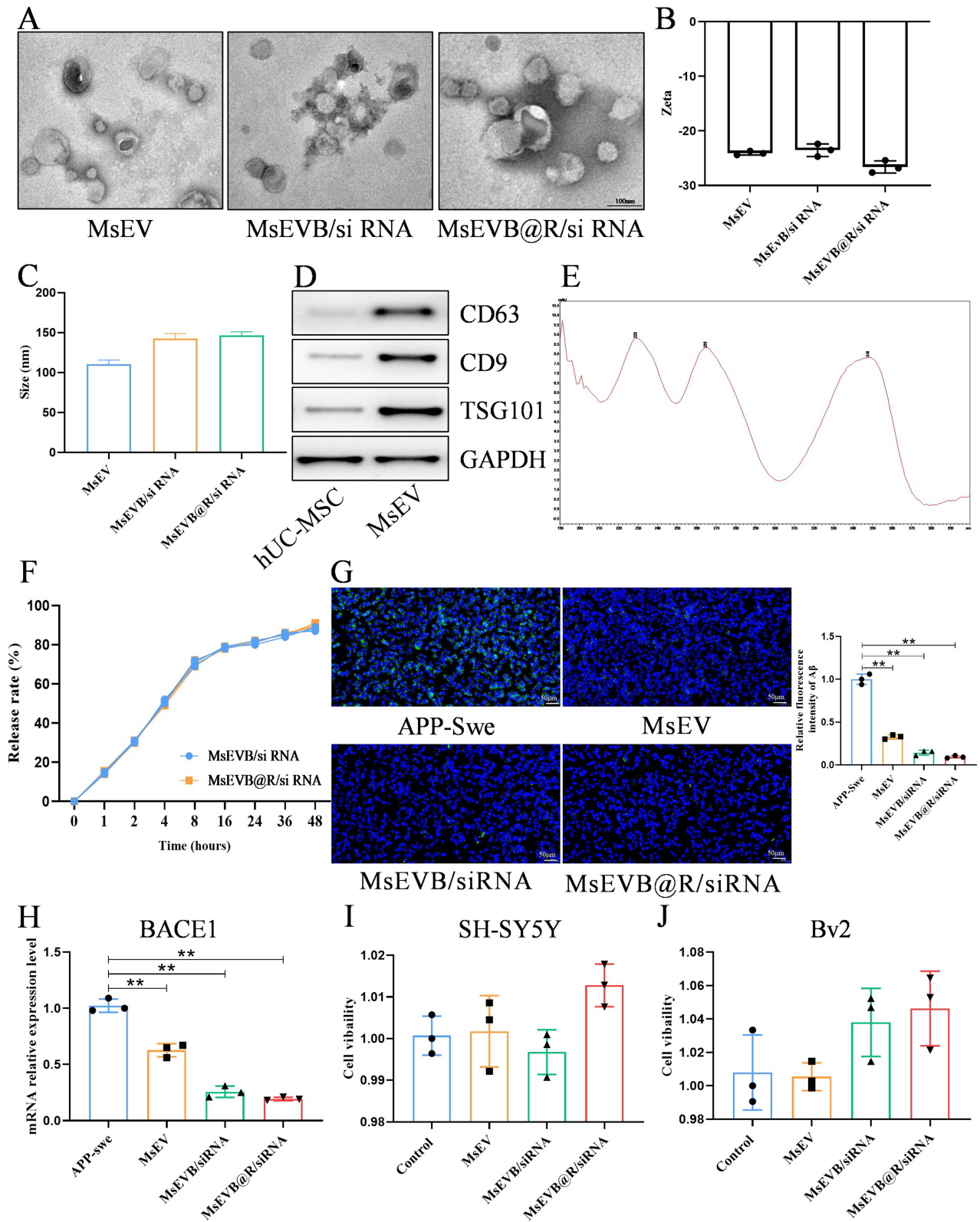


**Figure 1** Preparation and identification of hUC-MSC engineered exosomes. **(A)** Representative TEM images of MsEVB@R/siRNA (Scale bar: 100 nm). **(B)** Zeta potentials of MsEV, MsEVB/siRNA, and MsEVB@R/siRNA were analyzed by DLS. **(C)** Particle size of MsEVB@R/siRNA analyzed by DLS. **(D)** Protein expression levels of exosome markers CD63, CD9, TSG101, and GAPDH detected by Western blot (n = 3). **(E)** MsEVB@R/siRNA measured by spectrophotometer at 345 nm wavelength (n = 3). **(F)** In vitro drug release from different formulations (n = 3). **(G)** MsEV, MsEVB/siRNA and MsEVB@R/siRNA on Aβ protein expression in SH-SY5Y cells overexpressing APP gene measured by immunofluorescence and quantitative analysis (Scale bar: 50 μm, n = 3) (DAPI: Blue fluorescence; Aβ: Green fluorescence). **(H)** Relative expression of BACE1 mRNA in SH-SY5Y cells overexpressing APP gene after intervention by MsEV, MsEVB/siRNA, and MsEV@BBR/siRNA (n = 3). **(I and J)** Cell viability of SH-SY5Y cells and BV2 cells measured by CCK8 after incubation with MsEV, MsEVB/siRNA and MsEVB@R/siRNA for 24 h (n = 3). Data were presented as mean ± SD. \*\*p < 0.01.

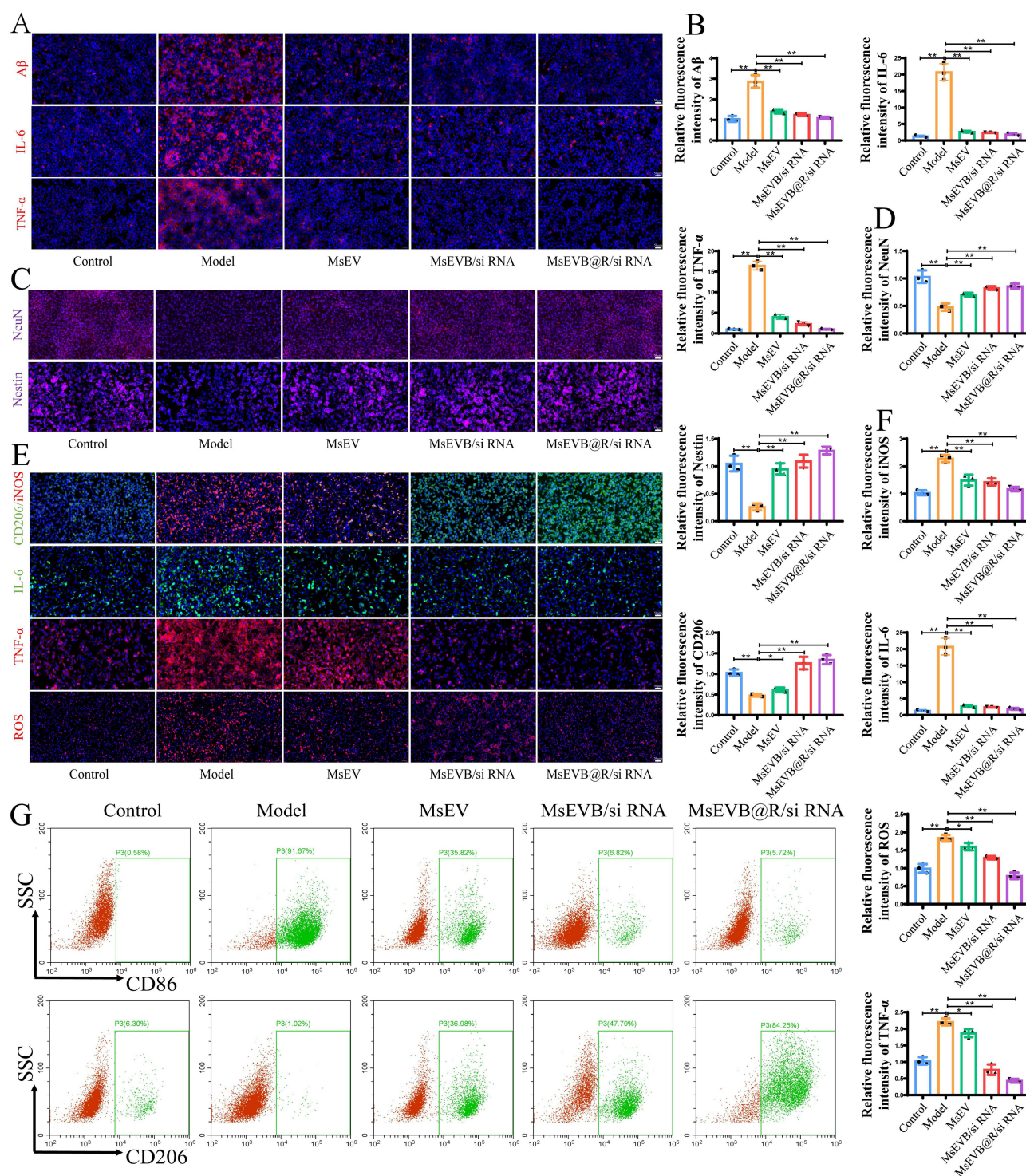


**Figure 2** Engineered hUC-MSC exosomes can effectively reduce nerve injury and suppress microglial inflammatory responses. **(A)** A $\beta$  deposition, IL-6, and TNF- $\alpha$  in SH-SY5Y cells after different formulations treatment was detected by immunofluorescence (Scale bar: 50  $\mu$ m). **(B)** Quantitative analysis of A $\beta$ , IL-6, and TNF- $\alpha$  expression levels in SH-SY5Y cells (n = 3). **(C)** NeuN and Nestin protein in SH-SY5Y cells after different formulations treatment was detected by immunofluorescence (Scale bar: 50  $\mu$ m). **(D)** Quantitative analysis of NeuN and Nestin protein expression levels in SH-SY5Y cells (n = 3). **(E)** iNOS, CD206, IL-6, TNF- $\alpha$ , and ROS in BV2 cells after treatment with different formulations were detected by immunofluorescence (Scale bar: 50  $\mu$ m). **(F)** Quantitative analysis of iNOS, CD206, IL-6, TNF- $\alpha$ , and ROS expression levels in BV2 cells (n = 3). **(G)** Flow cytometry analysis of CD86 and CD206 positive microglia with different experimental treatments. Data were presented as mean  $\pm$  SD. \* $p$  < 0.05, \*\* $p$  < 0.01.

inhibited, the inflammatory response was alleviated (Figures 2A and B; S3A–C). Concurrently, the expression levels of NeuN and Nestin proteins in the MsEVB@R/siRNA groups were significantly higher (Figures 2C and D; S3D and E). Berberine is an effective anti-inflammatory drug, exerting a strong therapeutic effect on neuroinflammation.<sup>30</sup> Inducible

nitric oxide synthase (iNOS) is an inflammatory marker of microglia M1, and CD206 is an inflammatory marker of microglia M2.<sup>31</sup> After A $\beta$  stimulation, the microglia entered a pro-inflammatory state. The expression level of the iNOS protein increased significantly, whereas the expression level of the CD206 protein decreased. Compared with the Model group, after treatment with MsEV, MsEVB/siRNA, and MsEVB@R/siRNA, the expression level of iNOS decreased, and that of CD206 increased in all groups, and the MsEVB@R/siRNA group was the most significant (Figures 2E and F; S4A). Concurrently, IL-6 and TNF- $\alpha$  protein expression was significantly inhibited, and the inflammatory response was alleviated in the MsEVB@R/siRNA group. The ROS expression level in the model group increased significantly upon A $\beta$  stimulation and decreased significantly after MsEVB@R/siRNA treatment (Figures 2E and F; S4B–D). To further evaluate whether MsEVB@R/siRNA could reduce the percentage of M1 microglia, we measured the amounts of M1 and M2 by flow cytometry (Figure 2G). Flow cytometry results showed that after treatment with MsEVB@R/siRNA, CD86-positive microglia significantly decreased and CD206-positive microglia significantly increased compared with the model group (Figure S2B). These results suggested that engineered exosomes can alter the state of microglia and reduce inflammation.

## MsEVB@R/siRNA Effectively Transduces siBACE1 and Berberine to Nerve Cells and Microglia in AD Mice

Nasal delivery is an effective method for the delivery of drugs, which can then directly enter the brain through the olfactory nerve and trigeminal nerve. Stem cell exosomes have low immunogenicity and can help reduce the removal of exosomes by the immune system and prolong action time.<sup>32</sup> Therefore, we studied their biological distribution and aggregation in the brain in vivo. The fluorescence intensity of MsEV, MsEVB/siRNA, and MsEVB@R/siRNA was significantly enhanced after 1 h, remained substantial after 6 h, and could still be observed in the brain after 24 h, with no significant difference in fluorescence intensity observed among the three groups (Figure 3A and B). Concurrently, the mice were sacrificed, and the fluorescence intensity of the organs and brain was further examined. After the drugs were loaded, no significant change was observed in the aggregation of the drugs in the brain tissues in the MsEVB/siRNA and MsEVB@R/siRNA groups, indicating that ultrasound did not affect the accumulation of exosomes in the brain (Figure 3C and D). Compared with that in the control group, after 6 h, the exosomes primarily accumulated in the brain. Fluorescence distribution was also observed in other organs, with observable accumulation in the liver and lungs (Figure S5A). Next, we analyzed the distribution of exosomes in the brain. First, we detected Cy5-MsEVB@R/siRNA in the olfactory bulb, suggesting that exosomes may enter the olfactory bulb via the olfactory nerve and then enter the hippocampus (Figures 3E and S5B). We analyzed the distribution of exosomes in the hippocampus and cerebral cortex. Colocalization results showed that the microglia primarily clustered around A $\beta$  plaques, and the fluorescence signals of MsEVB@R/siRNA overlapped with those of the microglia after the components entered the brain, indicating that MsEVB@R/siRNA could be taken up by the microglia and play a role (Figures 3F and S5C). Similarly, NeuN and MsEVB@R/siRNA showed that exosomes can be taken up by neuronal cells (Figures 3G and S5D).

## MsEVB@R/siRNA Improves Cognitive Behavior in AD Mice

Next, we assessed spatial learning and memory in mice using the MWM experiment. As illustrated in Figure 4A, the MsEV, MsEVB/siRNA, and MsEVB@R/siRNA groups exhibited a slight modification in escape latency during the 5d training period. Compared with that in the normal saline group, the learning performance of mice in the MsEVB@R/siRNA group was significantly better, the time to find the platform was significantly lower, and the average speed was significantly greater (Figure 4B–E). The test results on the last day indicated that the number of times the mice crossed the platform within 1 min was significantly greater in the MsEV, MsEVB/siRNA, and MsEVB@R/siRNA groups. Mice from the MsEVB@R/siRNA group had the highest frequency of crossing the platform (Figure 4F and H). In the experiment involving new and old object recognition, the percentage of mice touching new objects and old objects within 6 min was recorded. Compared with those in the MsEV and MsEVB/siRNA groups, mice in the MsEVB@R/siRNA group had the most frequent contact with new objects. Notably, the percentage of exposure to new objects and total exposure in the MsEVB@R/siRNA group was 20% higher than in the saline group (Figure 4G). Our results suggested that MsEVB@R/siRNA can significantly improve learning and space exploration.

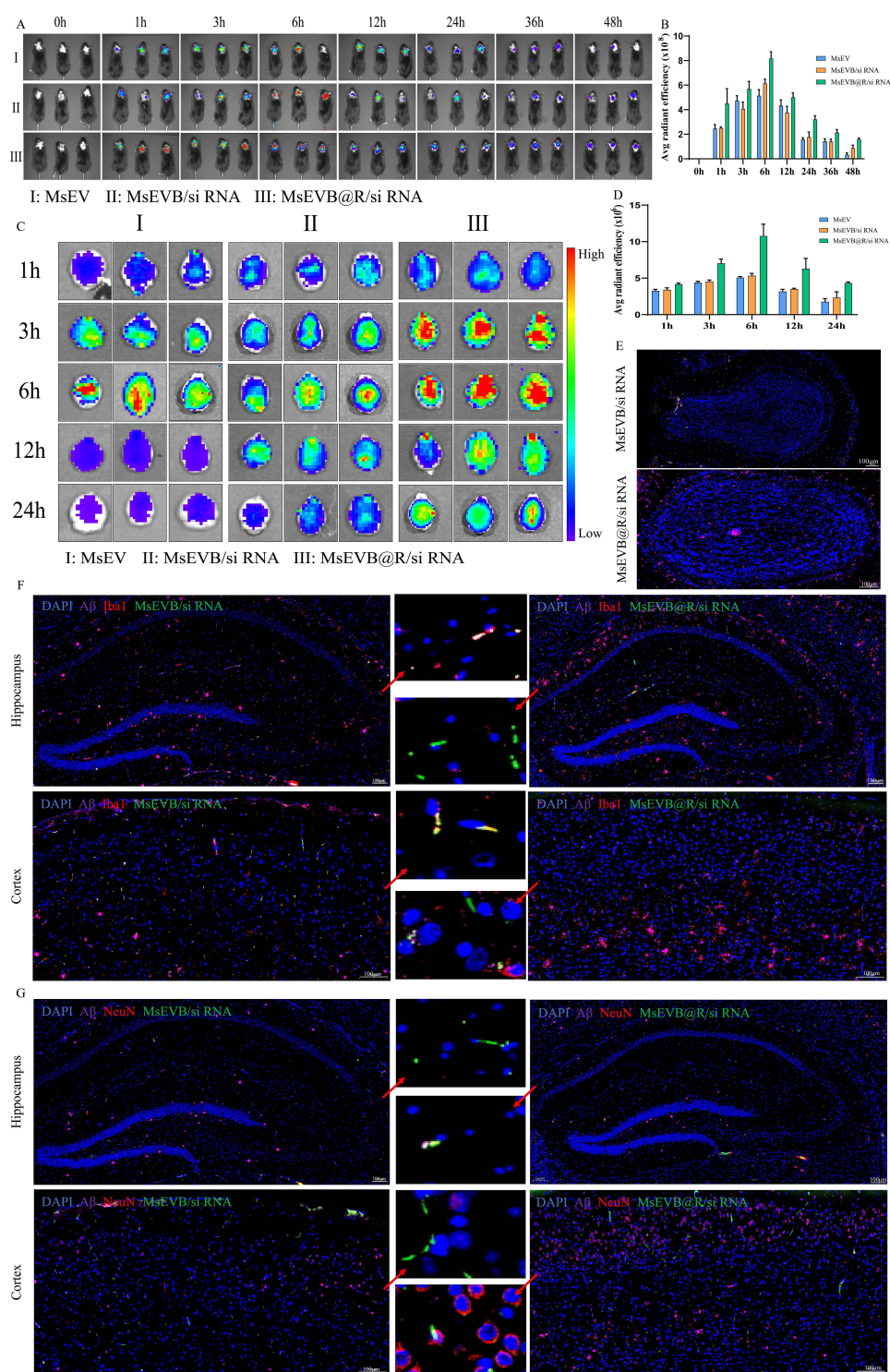


**Figure 3** MsEVB@R/siRNA effectively transduces siBACE1 and berberine to nerve cells and microglia in AD mice. **(A)** The distribution of fluorescence signal in the brain of 5xFAD mice was observed at 0, 1, 3, 6, 12, and 24 h after nasal infusion of MsEV, MsEVB/siRNA, and MsEVB@R/siRNA. **(B)** Quantitative analysis of fluorescent signals in mouse brain ( $n = 3$ ). **(C)** Fluorescence intensity in brain tissue of 5xFAD mice after 1, 3, 6, 12, and 24 h after nasal infusion of MsEV, MsEVB/siRNA, and MsEVB@R/siRNA was collected. **(D)** Quantitative analysis of fluorescent signals in brain tissue of 5xFAD mice ( $n = 3$ ). **(E)** Distribution of fluorescent signal in olfactory bulb of 5xFAD mice after 6 h after nasal infusion of MsEVB@R/siRNA (Scale bar: 100  $\mu\text{m}$ ) (DAPI: Blue fluorescence; MsEVB@R/siRNA: Red fluorescence). **(F)** Colocalized distribution of A $\beta$ , Iba1, and MsEVB@R/siRNA in hippocampus and cortex of 5xFAD mice 6 h after nasal infusion of MsEVB@R/siRNA (Scale bar: 100  $\mu\text{m}$ ) (DAPI: Blue fluorescence; A $\beta$ : Pink fluorescence; Iba1: Red fluorescence; MsEVB@R/siRNA: Green fluorescence). **(G)** Colocalized distribution of A $\beta$ , NeuN, and MsEVB@R/siRNA in hippocampus and cortex of 5xFAD mice 6 h after nasal infusion of MsEVB@R/siRNA (Scale bar: 100  $\mu\text{m}$ ) (DAPI: Blue fluorescence; A $\beta$ : Pink fluorescence; NeuN: Red fluorescence; MsEVB@R/siRNA: Green fluorescence). Data were presented as mean  $\pm$  SD.

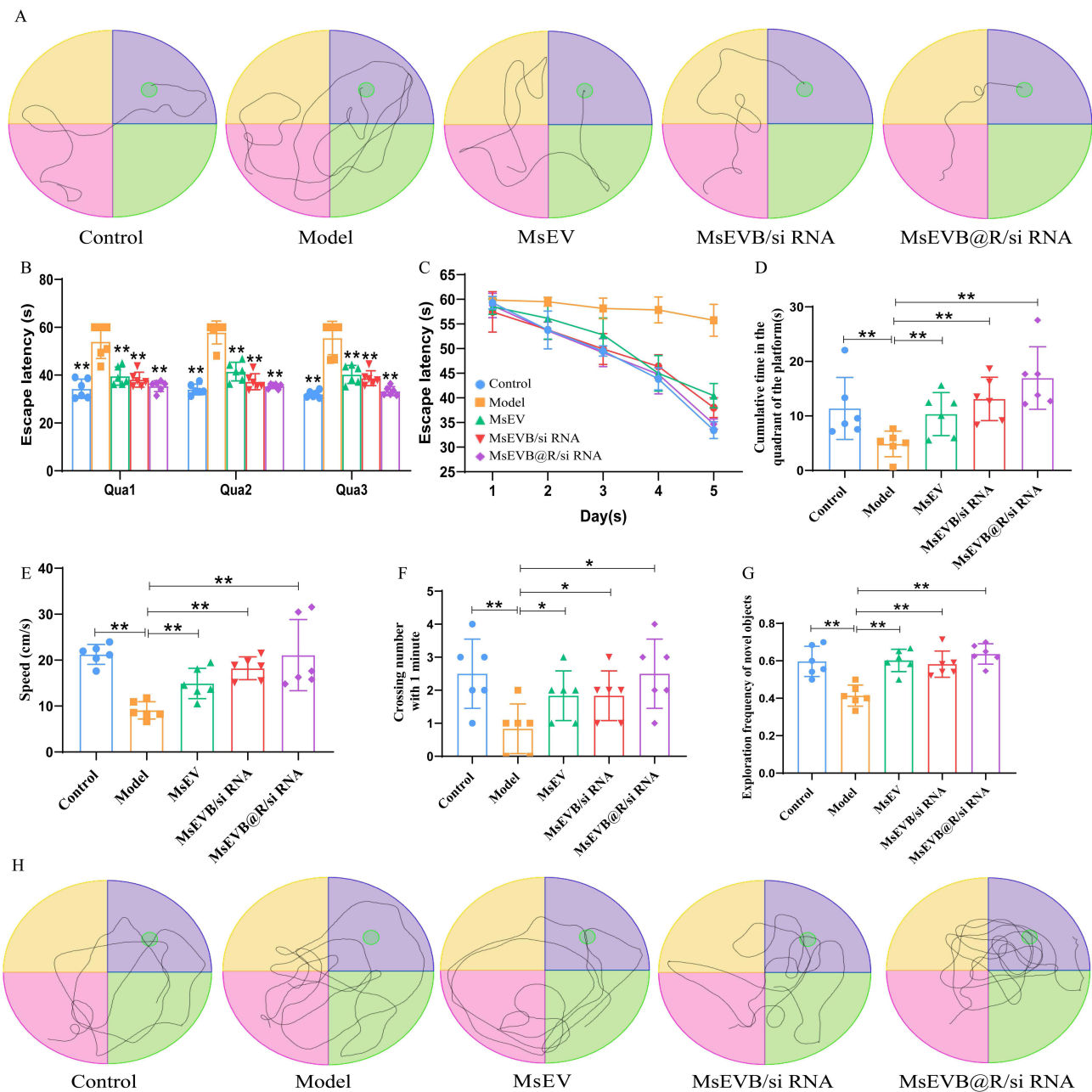


**Figure 4** MsEVB@R/siRNA improves cognitive behavior in AD mice. **(A)** The platform roadmap and heat map were searched for on the 5th day of water maze training ( $n = 6$ ). **(B)** Average time to find the platform in each quadrant on the 5th day. **(C)** Average time to find the platform on the 1st to 5th day. **(D)** Cumulative time in the platform quadrant on the 5th day. **(E)** Average swimming speed of 5xFAD mice on the 5th day. **(F)** Number of times that 5xFAD mice crossed the platform within 1 min on the 6th day. **(G)** Percentage of frequency of exploring new objects in total frequency during old and new object recognition training ( $n = 6$ ). **(H)** Road map and heat map of times of crossing the platform on the 6th day of water maze training ( $n = 6$ ). Data were presented as mean  $\pm$  SD. \* $p < 0.05$ , \*\* $p < 0.01$ .

## Effects of MsEVB@R/siRNA on the Transcriptomics of Brain Tissues in AD Mice

Next, we explored the impact of MsEVB@R/siRNA on AD expression through transcriptomic analysis and analyzed the mRNA expression of brain tissue in AD mice following MsEVB@R/siRNA treatment. In PCA results and heat map analysis, a significant cluster was observed in samples from the 5xFAD group and MsEVB@R/siRNA group, indicating differences in transcriptomic results between the two groups in response to drug intervention (Figure 5A and B). A total of 181 differentially expressed genes (DEGs) were detected. Compared with the 5xFAD group, the MsEVB@R/siRNA treatment upregulated 120 genes and 61 genes were downregulated. Volcano plots showed that compared with that in the

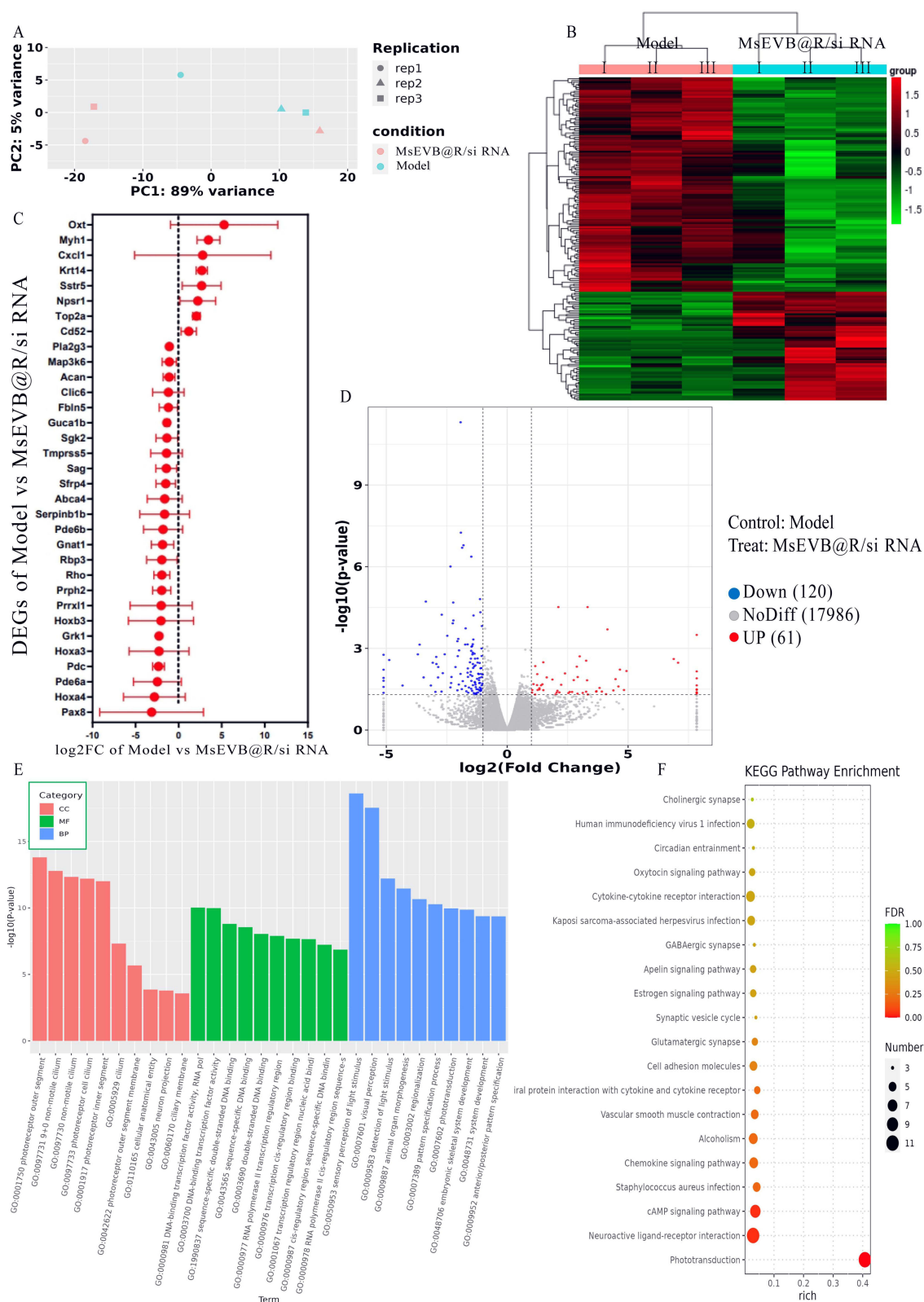


**Figure 5** Effects of MsEVB@R/siRNA on the transcriptomics of brain tissues in AD mice. **(A)** Principal component analysis (PCA) of gut microbiota after giving MsEVB@R/siRNA. **(B)** Model and MsEVB@R/siRNA group differential gene statistical map. **(C)** Log<sub>2</sub> fold change and 95% confidence interval of the 33 shared DEGs among brain tissues. **(D)** Volcanic map shows different metabolites in brain tissues between model and MsEVB@R/siRNA group. **(E)** GO analysis of differential gene enrichment in Model and MsEVB@R/siRNA groups. **(F)** KEGG analysis of differential gene enrichment in Model and MsEVB@R/siRNA groups. Data were presented as mean ± SD.

5xFAD group, 181 differentially expressed genes were detected in the MsEVB@R/siRNA group, of which 120 were downregulated and 61 were upregulated. The mRNA expression of Rho, Hoxa3, Hoxb3, Prrxl1, Serpinb1b, Pla2g3, Map3k6, Tmprss5, Sgk2, Sfrp4, and Guca1b genes was significantly downregulated. The mRNA expression of Oxt, Sstr5, Npsr1, Cd52, and Cxcl1, among other genes, was significantly upregulated (Figures 5C and D; S6A). We performed GO analyses to understand the differential DEG's genetic function, localization, and biological function. MsEVB@R/siRNA primarily regulated biological processes such as antigen processing and presentation of exogenous antigen, CCR6 chemokine receptor binding, chemokine activity, chemokine receptor binding, cytosolic ribosome, and dendritic spine morphogenesis (Figures 5E; S6B and C). In addition, KEGG pathway analysis revealed that DEGs involved a large number of regulatory horizontal pathways, including ABC transporters, antigen processing and presentation, B cell receptor signaling pathway, chemokine signaling pathway, dopaminergic synapse, and ECM-receptor interaction, to regulate AD (Figures 5F; S6D and E). These results suggest that MsEVB@R/siRNA may improve the symptoms of AD mice by regulating the above signaling pathways.

## MsEVB@R/siRNA Effectively Alleviates A $\beta$ Deposition, Inflammation, and Nerve Damage in AD Mice

Based on the therapeutic effect of MsEVB@R/siRNA in vitro, we further investigated their therapeutic effects on 5xFAD model mice. We found that the hippocampus and brain cortex of 6-month-old 5xFAD mice showed obvious A $\beta$  plaque deposition, whereas mice from the MsEV, MsEVB/siRNA, and MsEVB@R/siRNA groups showed lower levels of A $\beta$  aggregation in the brain, and the MsEVB@R/siRNA group showed the best therapeutic results (Figures 6A, B; S7A–C). Immunohistochemical results showed that compared with that in the control group, the Microtubule Associated Protein 2 (MAP2) expression levels was significantly decreased in the hippocampal and cortical areas of mice in the model group, and MAP2 expression levels were significantly increased in all groups after treatment (Figures 6C, D and S7D, E).

To confirm that optimized MsEVB@R/siRNA can promote the polarization of M1 to M2 phenotype, we evaluated the expression of representative iNOS and CD206 proteins. The expression level of iNOS in the cerebral cortex and hippocampus of the model group was significantly increased compared to the control group, while the expression of CD206 was significantly decreased. After treatment with MsEVB@R/siRNA, the expression level of CD206 was significantly increased compared to the model group, while the expression of iNOS was significantly decreased (Figures 6E–G; S7F and G). Meanwhile, compared with the model group, the pro-inflammatory factors TNF- $\alpha$  and IL-6 were significantly down-regulated after treatment with MsEVB@R/siRNA, indicating that the material had an inflammatory inhibitory effect. Whereas the anti-inflammatory factors IL-10 and IL-4 were significantly up-regulated (Figure 6H), indicating that it effectively promoted the transformation of macrophages from the M1 phenotype to the M2 phenotype. These results demonstrated an integrated systematic modification that binds stem cell exosomes, berberine, and siRNA with targeted peptides to regulate immune activity, reduced inflammation, released repair factors, and promoted transformation into a remodeling phase.

MsEVB@R/siRNA could significantly reduce A $\beta$  aggregation and neuroinflammation in the brain of mice and repair damaged neurons. Since a part of MsEVB@R/siRNA delivered via the nasal cavity entered different organs and the blood circulation, we performed HE staining of the heart, liver, spleen, lung, and kidney tissues. We did not observe obvious organic lesions in any organs after treatment with MsEV, MsEVB/siRNA, and MsEVB@R/siRNA (Figure S6F).

## Discussion

With the aging of the global population, the number of patients with AD is increasing. Reducing the global burden of AD and the severity of symptoms in affected patients is critical. AD is characterized by amyloid-beta plaque deposition, hyperphosphorylation of tau protein, and neuroinflammation leading to the development of typical and unique clinical symptoms.<sup>33,34</sup> Concerning therapeutic interventions, drugs currently approved by the US Food and Drug Administration (FDA) for the treatment of patients with AD, such as memantine and donepezil, can help improve the quality of life and prolong life expectancy but cannot stop AD development.<sup>35,36</sup> New therapeutic approaches are needed for AD treatment.

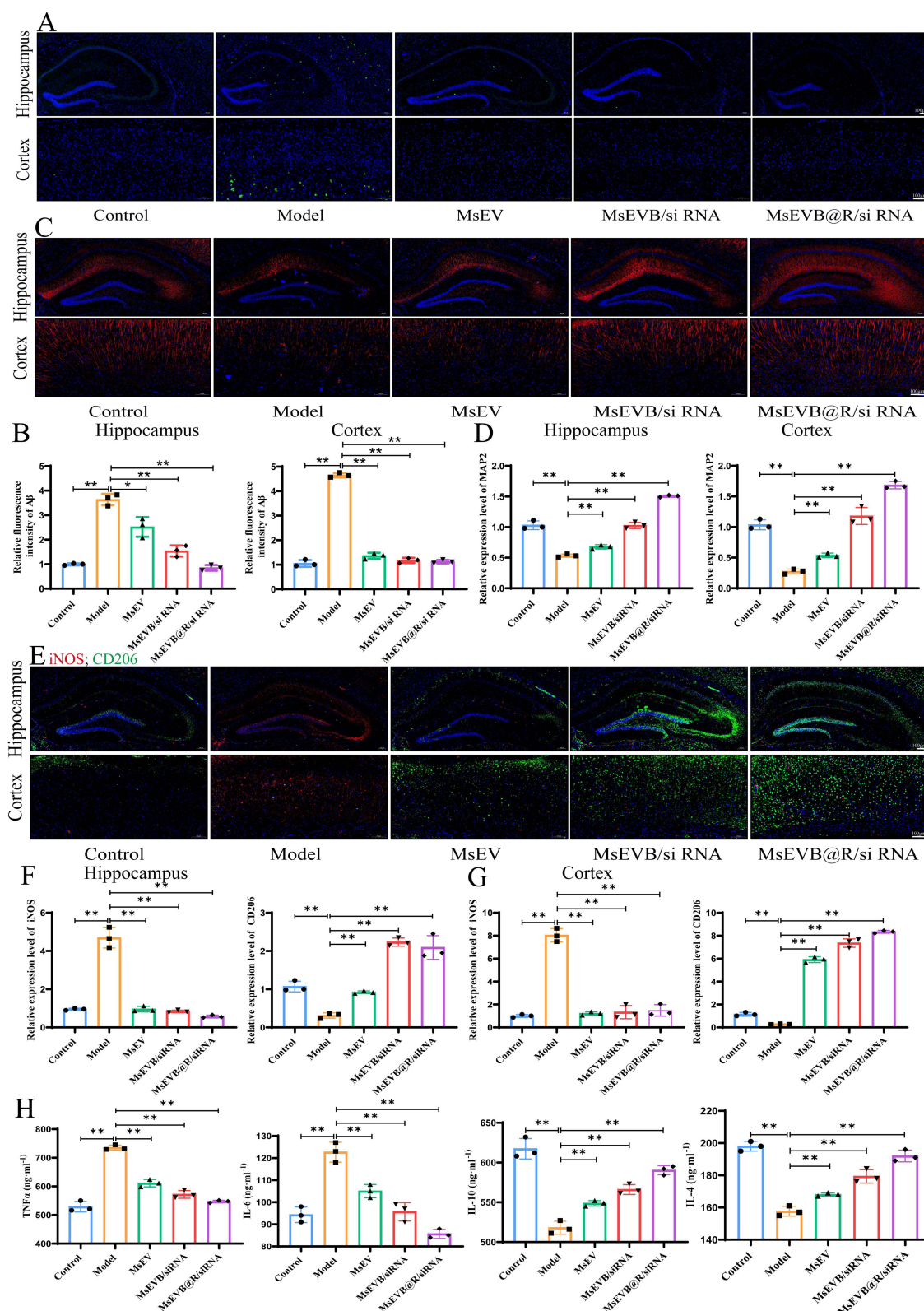


**Figure 6** MseVB@R/siRNA effectively alleviates A $\beta$  deposition, inflammation, and nerve damage in AD mice. **(A and B)** Immunofluorescence was used to detect A $\beta$  deposition levels in hippocampus and cortex of 5xFAD mice treated with different formulations, quantitative analysis was performed (Scale: 100  $\mu$ m) (DAPI: Blue fluorescence; A $\beta$ : Green fluorescence) (n = 3). **(C and D)** Immunofluorescence was used to detect MAP2 levels in hippocampus and cortex of 5xFAD mice treated with different formulations, quantitative analysis was performed (Scale: 100  $\mu$ m) (DAPI: Blue fluorescence; MAP2: Red fluorescence) (n = 3). **(E–G)** Immunofluorescence was used to detect iNOS and CD206 levels in hippocampus and cortex of 5xFAD mice treated with different formulations, quantitative analysis was performed (Scale: 100  $\mu$ m) (DAPI: Blue fluorescence; iNOS: Red fluorescence; CD206: Green fluorescence) (n = 3). **(H)** TNF- $\alpha$ , IL-6, IL-10 and IL-4 in brain tissue of mice were detected by ELISA (n = 3). Data were presented as mean  $\pm$  SD. \* $p$  < 0.05, \*\* $p$  < 0.01.

When developing new therapeutic interventions to treat AD, the low permeability of the BBB, which prevents hydrophobic therapeutic drugs from entering the brain, is an important consideration. Interestingly, our target drug, berberine, a natural anti-inflammatory drug, showed effective results in the treatment of AD. Even then, its delivery to the brain is challenging. Berberine has low bioavailability and can cause disturbances in the intestinal flora.<sup>30</sup> Therefore, an appropriate vector is needed to facilitate the delivery of berberine for potential AD treatment.

The BBB is an important structure that prevents the entry of drugs into the brain.<sup>37</sup> This affects the drug's action on the target and the drug utilization rate. Therefore, the route of administration is also a point of concern. The BBB is leaky in patients with AD, a phenomenon that is linked with cognitive decline. Thus, an impaired BBB may be an important component contributing to the onset of AD.<sup>38</sup> Several groups have reported the ability of exosomes to cross the BBB in vivo models of various diseases.<sup>39,40</sup> We previously measured the concentration of exosomes delivered via intravenous and nasal injection in the brain. The concentration of exosomes delivered by nasal delivery was higher in the brain, whereas the concentration of exosomes injected via the meridian in the brain was also higher in the liver and kidney, which we speculated might be related to the metabolism of exosomes in vivo. The nasal drug delivery route is a practical and non-invasive method to bypass the BBB and deliver therapeutic drugs to the brain via the olfactory and trigeminal nerves. Intranasal administration not only enhances drug delivery efficiency and reduces medication costs, but also decreases the requirement for long-term clinical care and shortens hospitalization duration, thereby alleviating strain on healthcare resources. Concurrently, this approach prolongs patients' occupational capacity, mitigates familial caregiving burdens, and diminishes reliance on social welfare systems. Furthermore, it improves patient dignity and quality of life while promoting advancements in the biopharmaceutical industry.

In recent years, stem cell exosomes have garnered considerable attention as drug carriers because they have low immunogenicity and function as stem cells, participating in intracellular communication by carrying various cargo, including nucleic acids and proteins.<sup>41</sup> The good drug-carrying properties of exosomes are significant, and modifications do not alter the function and structure of the exosomes.<sup>42,43</sup> A $\beta$ , produced by the cleavage of APP, is expressed at high levels in the brains of patients with AD and aggregates into toxic oligomers and fibers. These aggregates trigger chain of events that lead to neuronal damage and necrosis.<sup>29,44</sup> Here, to reduce A $\beta$  deposition and treat neuroinflammation in AD, we constructed Exos loaded with BACE1 siRNA and berberine and modified it with brain-targeting peptide RVG29 for intranasal delivery into the brain. BACE1 siRNA and berberine were introduced into Exos by ultrasound and then incubated at 37°C to restore the Exos membrane to normal. RVG29 is a rabies virus polypeptide with 29 amino acids that specifically binds to the acetylcholine receptor (nAChR) expressed in BBB and neuronal cells. MsEVB@R/siRNA was identified and mapped by transmission electron microscopy, Western blotting, proteomic analysis, and transcriptome sequencing. After MsEVB@R/siRNA was delivered via the nasal route, we investigated the distribution of MsEVB@R/siRNA in the brain and different organs and compared the effects of MsEV, MsEVB/siRNA, and MsEVB@R/siRNA on behavior, neurostructural repair, and neuroinflammation. After treatment, we analyzed changes in inflammatory signals and gene expression in AD and discussed the potential mechanism.

After MsEVB@R/siRNA was delivered into the brain through the nasal cavity, MsEVB@R/siRNA was taken up by neuronal cells and microglia, and APP was used as a targeted receptor. First, BACE1 siRNA downregulated the expression of  $\beta$ -secreting enzyme and reduced the production of A $\beta$  from the source. Following this, berberine suppressed the inflammatory response in the microglia. Exosomes altered the state of the microglia from pro-inflammatory to anti-inflammatory, promoted the uptake of extracellular A $\beta$  by microglia, and reduced the deposition of A $\beta$ . Exosomes also repaired damaged neurons, improved cognitive dysfunction, and alleviated AD symptoms. Thus far, we have learned that MsEVB@R/siRNA is efficiently delivered to APP-overexpressing nerve cells and microglia. However, to further determine if it can improve AD pathogenesis, we must examine the effects of MsEVB@R/siRNA on cognitive and motor behavior in a 5xFAD mouse model. The results of behavioral experiments, such as the MWM experiment and new and old object recognition tests, showed that MsEVB@R/siRNA improved cognitive function in AD mice (Figure 3). Brain tissue transcriptomics further shed light on the possible signaling pathway of MsEVB@R/siRNA for AD remission. Upregulated differentially expressed genes are closely related to chemotactic response. Meanwhile, GO analysis indicated that MsEVB@R/siRNA may participate in inflammatory response through chemokine activity and

chemokine receptor binding. The results indicated that exosomes primarily regulate neuroinflammation, the regulation of neuronal damage, and energy metabolism, which are closely related to the progression of AD.

Overall, the exosome-based engineered targeted drug delivery demonstrated in this study may also be applicable to other brain diseases, such as glioma, Parkinson's disease, and amyotrophic lateral sclerosis. While stem cells have been widely used as a source of exosomes and their genetic engineering, several other cell types, such as macrophages, could also be explored as potential sources for the effective targeted delivery of exosomes. As a payload, several other drugs and combinations may be loaded into exosomes for delivery to the brain. Although our findings revealed the potential of designing innovative drug delivery systems for the brain using exosomes derived from umbilical cord stem cells, further investigation was needed. For the effective application of exosomes, the potential route of nasal delivery of exosomes through the olfactory region to the brain must be investigated. In addition, it is worth investigating the specific mechanism of action of exosome-based engineering delivery systems and the feasibility of clinical treatment and potential side effects. Current preservation protocols for exosomes primarily rely on storage at  $-80^{\circ}\text{C}$ , yet prolonged storage may induce structural alterations that compromise functional integrity. Furthermore, such cryogenic conditions pose significant challenges for long-distance transportation. To address this issue, we propose implementing lyophilization (freeze-drying) of exosomes in subsequent studies, which enhances preservation stability and facilitates transportation. Prior to each application, the lyophilized exosomes can be reconstituted with PBS or sterile water for subsequent administration.

## Conclusion

In conclusion, a multifunctional Exos (MsEVB@R/siRNA) was successfully prepared to enhance AD. MsEVB@R/siRNA was efficiently delivered to APP-overexpressing nerve cells and microglia. Berberine effectively suppressed the release of inflammatory factors, thereby reducing neuroinflammation. Exosomes altered the state of the microglia from pro-inflammatory to anti-inflammatory and reduced the deposition of A $\beta$  by promoting the uptake of extracellular A $\beta$ , and also repaired damaged neurons and improved cognitive dysfunction. In conclusion, MsEVB@R/siRNA had good effects on clearing A $\beta$  deposition, reducing inflammation, and relieving AD and had great application potential the in treatment of Alzheimer's disease.

## Ethics Approval and Consent to Participate

Animal experiments were conducted according to the guidelines established and approved by the Laboratory Animal Management Committee of Yunnan Best Biotech Co., LTD. The assigned approval number is BST-MICE-PZ-20230609-1.

## Acknowledgments

The financial support provided by the grants from the National Natural Science Foundation of China (32300682 to C.X.), the Fundamental Research Funds for the Central Universities (FRF-TP-22-007A1 to C.X.).

## Author Contributions

All authors made a significant contribution to the work reported, whether that is in the conception, study design, execution, acquisition of data, analysis and interpretation, or in all these areas; took part in drafting, revising or critically reviewing the article; gave final approval of the version to be published; have agreed on the journal to which the article has been submitted; and agree to be accountable for all aspects of the work.

## Disclosure

The author(s) report no conflicts of interest in this work.

## References

1. Alzheimer's Association. Alzheimer's disease facts and figures. *Alzheimers Dement.* 2021;17(3):327–406. doi:10.1002/alz.12328
2. Scheltens P, De Strooper B, Kivipelto M, et al. Alzheimer's disease. *Lancet.* 2021;397(10284):1577–1590. doi:10.1016/S0140-6736(20)32205-4

3. Long JM, Holtzman DM. Alzheimer Disease: an Update on Pathobiology and Treatment Strategies. *Cell*. 2019;179(2):312–339. doi:10.1016/j.cell.2019.09.001
4. Yang X, Yang W, Xia X, et al. Intranasal Delivery of BACE1 siRNA and Rapamycin by Dual Targets Modified Nanoparticles for Alzheimer's Disease Therapy. *Small*. 2022;18(30):e2203182. doi:10.1002/sml.202203182
5. Jia J, Wei C, Chen S, et al. The cost of Alzheimer's disease in China and re-estimation of costs worldwide. *Alzheimers Dement*. 2018;14(4):483–491. doi:10.1016/j.jalz.2017.12.006
6. Gaikwad S, Senapati S, Haque MA, Kaye R. Senescence, brain inflammation, and oligomeric tau drive cognitive decline in Alzheimer's disease: evidence from clinical and preclinical studies. *Alzheimers Dement*. 2024;20(1):709–727. doi:10.1002/alz.13490
7. van Dyck CH, Swanson CJ, Aisen P, et al. Lecanemab in Early Alzheimer's Disease. *N Engl J Med*. 2023;388(1):9–21. doi:10.1056/NEJMoa2212948
8. Lei T, Yang Z, Xia X, et al. A nanocleaner specifically penetrates the blood–brain barrier at lesions to clean toxic proteins and regulate inflammation in Alzheimer's disease. *Acta Pharm Sin B*. 2021;11(12):4032–4044. doi:10.1016/j.apsb.2021.04.022
9. Leclerc M, Bourassa P, Vandal M, et al. Interactions between insulin, the blood-brain barrier, and beta-amyloid in Alzheimer's disease. *Alzheimer's Dementia*. 2020;16(S3):e039510. doi:10.1002/alz.039510
10. Tenchov R, Sasso JM, Wang X, Liaw WS, Chen CA, Zhou QA. Exosomes—Nature's Lipid Nanoparticles, a Rising Star in Drug Delivery and Diagnostics. *ACS Nano*. 2022;16(11):17802–17846. doi:10.1021/acsnano.2c08774
11. Liang Y, Duan L, Lu J, Xia J. Engineering exosomes for targeted drug delivery. *Theranostics*. 2021;11(7):3183–3195. doi:10.7150/thno.52570
12. Agrawal M, Saraf S, Saraf S, et al. Nose-to-brain drug delivery: an update on clinical challenges and progress towards approval of anti-Alzheimer drugs. *J Control Release*. 2018;281:139–177. doi:10.1016/j.jconrel.2018.05.011
13. Khan AR, Liu M, Khan MW, Zhai G. Progress in brain targeting drug delivery system by nasal route. *J Control Release*. 2017;268:364–389. doi:10.1016/j.jconrel.2017.09.001
14. Cheng L, Hill AF. Therapeutically harnessing extracellular vesicles. *Nat Rev Drug Discov*. 2022;21(5):379–399. doi:10.1038/s41573-022-00410-w
15. Lotfy A, AboQuella NM, Wang H. Mesenchymal stromal/stem cell (MSC)-derived exosomes in clinical trials. *Stem Cell Res Ther*. 2023;14(1):66. doi:10.1186/s13287-023-03287-7
16. Dixon AC, Dawson TR, Di Vizio D, Weaver AM. Context-specific regulation of extracellular vesicle biogenesis and cargo selection. *Nat Rev Mol Cell Biol*. 2023;24(7):454–476. doi:10.1038/s41580-023-00576-0
17. Zhai L, Shen H, Sheng Y, Guan Q. ADMSC Exo-MicroRNA-22 improve neurological function and neuroinflammation in mice with Alzheimer's disease. *J Cell Mol Med*. 2021;25(15):7513–7523. doi:10.1111/jcmm.16787
18. Wei H, Xu Y, Chen Q, Chen H, Zhu X, Li Y. Mesenchymal stem cell-derived exosomal miR-223 regulates neuronal cell apoptosis. *Cell Death Dis*. 2020;11(4):290. doi:10.1038/s41419-020-2490-4
19. Mowry FE, Espejo-Porras F, Jin S, et al. Chronic nSMase inhibition suppresses neuronal exosome spreading and sex-specifically attenuates amyloid pathology in APP knock-in Alzheimer's disease mice. *Neurobiol Dis*. 2023;184:106213. doi:10.1016/j.nbd.2023.106213
20. Lyu T, Zhang B, Li M, Jiao X, Song Y. Research progress on exosomes derived from mesenchymal stem cells in hematological malignancies. *Hematol Oncol*. 2021;39(2):162–169. doi:10.1002/hon.2793
21. Som Chaudhury S, Sinha K, Das Mukhopadhyay C. Intranasal route: the green corridor for Alzheimer's disease therapeutics. *J Drug Delivery Sci Technol*. 2021;66:102791. doi:10.1016/j.jddst.2021.102791
22. Micci MA, Krishnan B, Zhang W, et al. [o1–07–03]: synaptic Resilience to Tau and Amyloid Beta Oligomers Induced by Neural Stem Cell-Derived Exosomes. *Alzheimer's Dementia*. 2017;13(7S\_Part\_4):P205–P205. doi:10.1016/j.jalz.2017.07.072
23. Bellaver B, Povala G, Ferreira PCL, et al. Astrocyte reactivity influences amyloid- $\beta$  effects on tau pathology in preclinical Alzheimer's disease. *Nat Med*. 2023;29(7):1775–1781. doi:10.1038/s41591-023-02380-x
24. Zhao X, Sun J, Xiong L, et al.  $\beta$ -amyloid binds to microglia Dectin-1 to induce inflammatory response in the pathogenesis of Alzheimer's disease. *Int J Biol Sci*. 2023;19(10):3249–3265. doi:10.7150/ijbs.81900
25. Grubman A, Choo XY, Chew G, et al. Transcriptional signature in microglia associated with A $\beta$  plaque phagocytosis. *Nat Commun*. 2021;12(1):3015. doi:10.1038/s41467-021-23111-1
26. Sun C, Dong S, Chen W, Li J, Luo E, Ji J. Berberine alleviates Alzheimer's disease by regulating the gut microenvironment, restoring the gut barrier and brain-gut axis balance. *Phytomedicine*. 2024;129:155624. doi:10.1016/j.phymed.2024.155624
27. Shireby G, Dempster EL, Policicchio S, et al. DNA methylation signatures of Alzheimer's disease neuropathology in the cortex are primarily driven by variation in non-neuronal cell-types. *Nat Commun*. 2022;13(1):5620. doi:10.1038/s41467-022-33394-7
28. Rahbaran M, Zekiy AO, Bahramali M, et al. Therapeutic utility of mesenchymal stromal cell (MSC)-based approaches in chronic neurodegeneration: a glimpse into underlying mechanisms, current status, and prospects. *Cell Mol Biol Lett*. 2022;27(1):56. doi:10.1186/s11658-022-00359-z
29. Yan R, Vassar R. Targeting the  $\beta$  secretase BACE1 for Alzheimer's disease therapy. *Lancet Neurol*. 2014;13(3):319–329. doi:10.1016/S1474-4422(13)70276-X
30. Raju M, Kunde SS, Auti ST, Kulkarni YA, Wairkar S. Berberine loaded nanostructured lipid carrier for Alzheimer's disease: design, statistical optimization and enhanced in vivo performance. *Life Sci*. 2021;285:119990. doi:10.1016/j.lfs.2021.119990
31. Yang Y, Gao ZF, Hou GG, Meng QG, Hou Y. Discovery of anti-neuroinflammatory agents from 1,4,5,6-tetrahydrobenzo[2,3]oxepino[4,5-d]pyrimidin-2-amine derivatives by regulating microglia polarization. *Eur J Med Chem*. 2023;259:115688. doi:10.1016/j.ejmech.2023.115688
32. Jeong SH, Jang JH, Lee YB. Drug delivery to the brain via the nasal route of administration: exploration of key targets and major consideration factors. *J Pharm Investig*. 2023;53(1):119–152. doi:10.1007/s40005-022-00589-5
33. Malpetti M, Cope TE, Street D, et al. Microglial activation in the frontal cortex predicts cognitive decline in frontotemporal dementia. *Brain*. 2023;146(8):3221–3231. doi:10.1093/brain/awad078
34. Zenaro E, Pietronigro E, Bianca VD, et al. Neutrophils promote Alzheimer's disease-like pathology and cognitive decline via LFA-1 integrin. *Nat Med*. 2015;21(8):3913. doi:10.1038/nm.3913
35. Nirogi R, Goyal VK, Bhyrapuneni G, et al. Masupirdine in combination with donepezil and memantine in patients with moderate Alzheimer's disease: subgroup analyses of memantine regimen, plasma concentrations and duration of treatment. *Alzheimer's Dementia*. 2020;16(S9):e039254. doi:10.1002/alz.039254

36. Allsop D, Martin FL, Moore S, Fullwood NJ. Donepezil for severe Alzheimer's disease. *Lancet*. 2006;368(9533):9533:361. doi:10.1016/S0140-6736(06)69097-1
37. Terstappen GC, Meyer AH, Bell RD, Zhang W. Strategies for delivering therapeutics across the blood-brain barrier. *Nat Rev Drug Discov*. 2021;20(5):362–383. doi:10.1038/s41573-021-00139-y
38. Agrawal M, Ajazuddin, Tripathi DK, et al. Recent advancements in liposomes targeting strategies to cross blood-brain barrier (BBB) for the treatment of Alzheimer's disease. *J Control Release*. 2017;260:61–77. doi:10.1016/j.jconrel.2017.05.019
39. Felker J, Agnihotri S. Hurdling over the blood-brain barrier with exosome technology. *Neuro Oncol*. 2022;24(11):1884–1885. doi:10.1093/neuonc/ncac214
40. Liu X, Xia T, Fang Y, et al. Overcoming the blood-brain barrier by using a multistage exosome delivery system to inhibit central nervous system lymphoma. *Nanomedicine*. 2022;41:102523. doi:10.1016/j.nano.2022.102523
41. Jin X, Xia T, Luo S, Zhang Y, Xia Y, Yin H. Exosomal lipid PI4P regulates small extracellular vesicle secretion by modulating intraluminal vesicle formation. *J Extracell Vesicles*. 2023;12(4):e12319. doi:10.1002/jev2.12319
42. Sharma S, Masud MK, Kaneti YV, et al. Extracellular Vesicle Nanoarchitectonics for Novel Drug Delivery Applications. *Small*. 2021;17(42):e2102220. doi:10.1002/sml.202102220
43. Armstrong JPK, Stevens MM. Strategic design of extracellular vesicle drug delivery systems. *Adv Drug Deliv Rev*. 2018;130:12–16. doi:10.1016/j.addr.2018.06.017
44. Vincent B, Maitra S. BACE1-dependent metabolism of neuregulin 1: bridging the gap in explaining the occurrence of schizophrenia-like symptoms in Alzheimer's disease with psychosis? *Ageing Res Rev*. 2023;89:101988. doi:10.1016/j.arr.2023.101988

International Journal of Nanomedicine

Publish your work in this journal

The International Journal of Nanomedicine is an international, peer-reviewed journal focusing on the application of nanotechnology in diagnostics, therapeutics, and drug delivery systems throughout the biomedical field. This journal is indexed on PubMed Central, MedLine, CAS, SciSearch®, Current Contents®/Clinical Medicine, Journal Citation Reports/Science Edition, EMBase, Scopus and the Elsevier Bibliographic databases. The manuscript management system is completely online and includes a very quick and fair peer-review system, which is all easy to use. Visit <http://www.dovepress.com/testimonials.php> to read real quotes from published authors.

Submit your manuscript here: <https://www.dovepress.com/international-journal-of-nanomedicine-journal>

**Dovepress**  
Taylor & Francis Group